Journal of Applied Polymer Science

Synthesis, Characterization and Properties of Cellulose-Grafted Glycine Derivatives

Ming Guo,[1,2] Huan Wang,[1] Liping Sun,[3] Yanjun Li[2]
[1]Department of Chemistry, Zhejiang A & F University, Lin'an 311300, China
[2]National Engineering and Technology Research Center of Wood-Based Resources Comprehensive Utilization, Zhejiang A & F University, Lin'an Zhejiang 311300, China
[3]School of Environmental & Resource Sciences, Zhejiang A & F University, Lin'an 311300, China
Correspondence to: M. Guo (E-mail: tdky@hotmail.com)

ABSTRACT: Novel Schiff base cellulose derivatives were successfully prepared by a bridge-coupling reaction from dialdehyde cellulose (DAC), which was obtained by the selective oxidation of sodium periodate to cotton fibers, in which the glycine (Gly) was bonded onto the DAC chains by a Schiff base reaction with *p*-nitrobenzaldehyde as a bridge. The structures of the graft copolymer (DAC-*g*-Gly) were characterized by Fourier transform infrared spectroscopy, X-ray diffraction, solid-state NMR, and scanning electronic microscopy. The thermodynamic properties were analyzed by thermogravimetric analysis and differential scanning calorimetry, and the biodegradability was also tested by the microbial degradation and the active sludge method. The results indicate that Gly was connected to DAC by chemical bonding, which changed the thermal stability, and that DAC-*g*-Gly could be biodegraded significantly.
 J. Appl. Polym. Sci. **2014**, *131*, 40929.

KEYWORDS: biodegradable; biomaterials; cellulose and other wood products; grafting; thermal properties

Received 11 January 2014; accepted 18 April 2014
DOI: 10.1002/app.40929

INTRODUCTION

Chemically modified biodegradable cellulose-based materials are one kind of biomass-based biodegradable polymer materials that have broad prospects for development in biomass energy research.[1,2] Compared with synthetic materials, degradable cellulose-based materials have many advantages. First, there are many hydroxyl groups on the cellulose macromolecule; this leads to a stronger reactivity and interaction properties, so the process of such materials is relatively simple, low cost, and without pollution. Second, the material can be degraded by microorganisms or bacteria. Although traditional fossil-resource-based polymers are difficult to decompose in the natural environment, the secondary pollution caused by waste materials has become a worldwide public hazard. Cellulose-based biodegradable polymer materials are expected to become the new abundant and widely used polymer material.[3] Third, cellulose material itself is nontoxic. Therefore, cellulose-based materials will have potential applications. It is of significance to develop cellulose material as a matrix for biodegradable materials to protect environment, save resources, and promote the economy.

At present, researchers use chemical theory and technology to change the chemical structure of cellulose molecules by modification, restructuring, recombination, and so on. Various kinds of modification techniques have been used to change their specific properties.[4–6] Cellulose nanocrystals modified by grafting from L-lactide by ring-opening polymerization improved the compatibility of nanocrystals and hydrophobic polymer matrices.[7] The presence of carboxylic groups in the polymer chain modified the swelling properties of the material and the ability to bind cations through an ion-exchange mechanism involving —COOH groups.[8] Among these techniques, an important Schiff base reaction was involved. In recent years, many Schiff base derivatives have been obtained with the reaction of a primary amine in the macromolecular chain reacting with a variety of aldehydes. These Schiff bases are all of great importance in the fields of analytical chemistry, stereochemistry, electrochemistry, spectroscopy, molecular self-assembly, supermolecular chemistry, biochemistry model systems, catalysis, materials, nuclear chemistry, and chemical disciplines.[9–12] However, primary amines or aldehydes are not present in cellulose; cellulose has to be modified to obtain the Schiff base compounds. One effective method is through the selective oxidation of dialdehyde cellulose (DAC) with the use of a further reaction with amines to produce oxidative Schiff alkali cellulose derivatives. However, in the general reaction of the Schiff base, it is difficult to obtain stable Schiff base derivatives. It is necessary to introduce aromatic

compounds as a bridge graft to form a stable Schiff base compounds.[13] Currently, the research is still limited, and the literature has few reports. In this study, using the selective oxidation reaction of cotton fibers (CFs) to prepare DAC and then taking the DAC as a carrier and *p*-nitrobenzaldehyde (*p*-NBD) and glycine (Gly) as the grafting bridge and grafting branch, respectively, we synthesized new Schiff base derivatives of DAC-*g*-Gly with three-step synthesis methods. The new compound, which has not been previously reported, had a high stability. Meanwhile, we also characterized the synthetic product structures and tested the performance. Relevant work for the synthesis of such novel compounds can provide a useful reference.

EXPERIMENTAL

Materials and Reagents

The materials used included CFs (98.0% cellulose, XinYi Surgical Dressing Products Factory, Yancheng, China). The CFs were soaked in a 14% sodium hydroxide solution for 24 h, filtered, washed with distilled water to neutral, vacuum-dried at 60°C, pulverized for later use. We also used sodium periodate (analytically pure, $NaIO_4$; Zhejiang Quzhou Haichuan Chemicals Co., Ltd.), *p*-NBD (analytically pure, Shanghai Chemical Safety Nike), and Gly (analytically pure, Chemical Technology Co., Ltd., Shanghai Hanhong). Redistilled water (ddH_2O) was used throughout the experiments. All other chemicals were analytical grade and were used as received without further purification.

Synthesis of the DAC-Grafted Gly

Amounts of 10 mmol of Gly, 10 mmol of sodium hydroxide, and 50 mL of new distilled nonwater methanol were mixed into a 250-mL, three-necked flask at 50°C. An amount of 10 mmol of *p*-NBD was dissolved in 50 mL of anhydrous methanol, and then, it was slowly titrated into the mixed solution for a 1-h reaction by stirring. We rotary-evaporated the reaction solution until crystals appeared; these were filtered, washed with ether, and recrystallized with anhydrous ethanol. The yellow *p*-NBD–Gly–Schiff base solid was vacuum-dried at 50°C.

An amount of 10 mmol of *p*-NBD–Gly–Schiff base solid and 50 mL of new distilled nonwater methanol were added to a three-necked flask. We then added 10 mmol of zinc powder and 10 mmol of crystalline-state aluminum chloride successively at room temperature, stirred this solution to reflux for 5 h, filtered the solution and washed the filter cake several times with 0.01 mol/L hydrochloric acid, washed it two to three times with ethanol, vacuum-dried it at 60°C, and obtained the *p*-aminobenzaldehyde (*p*-ABD)–Gly–Schiff base.

The preparation of DAC and the determination of aldehyde were done in accordance with the literature.[14] The obtained DAC was ground into powder and vacuum-dried at 60°C. An amount of 2.00 g of DAC suspended in 150 mL of ddH_2O was added into a 250-mL, three-necked flask, in which 4.46 g of *p*-ABD–Gly–Schiff base was added. We stirred this at 50°C for 12 h, and 0.1 mol/L NaOH and glacial acetic acid were added to the mixture to adjust the pH to 5.0. The solution was filtered and washed with plenty of methanol several times until the *p*-ABD–Gly–Schiff base molecule could not be detected by thin-layer chromatography. The expected cellulose-grafted Gly (DAC-*g*-Gly) product was finally obtained after vacuum drying at 60°C.

Characterization of the Reactants, Intermediates, and Final Product

Fourier transform infrared (FTIR) spectra of the reactants, intermediates, and final product (DAC-*g*-Gly) were obtained with a spectrophotometer (Prestige-21, Shimadzu, Japan) with KBr pellets in the range 500–4000 cm^{-1}.

Cross-polarization (CP)/magic-angle spinning (MAS) ^{13}C-NMR spectra of the reactants, intermediates, and final products were recorded on an Avance II/400-MHz NMR spectrometer (Bruker, Switzerland). The test conditions were as follows: MAS speed = 3.8 MHz, ^{13}C observation frequency = 75 MHz; 8192 data points, 696 scans, amino acid internal standard, resolution = 4.88 Hz, four pulse sequences ($PS_1 = 5.00$ μs, $PS_2 = 2000.00$ μs, $PS_3 = 5.00$ μs, and $PS_4 = 500.00$ μs), four pulse intervals ($PI_1 = 10.00$ 00 ms, $PI_2 = PI_3 = 10.0000$ ms, and $PI_4 = 1.0000$ ms), and pulse delay time = 12.00 s.

X-ray diffraction (XRD) patterns of the reactants, intermediates, and final products were measured by a XRD6000 powder diffractometer (Shimadzu, Japan), and we used a Cu target at 35 kV and 30 mA. The relative intensity was recorded in the scattering range (2θ) of 4–50°. The apparent morphologies of the reactants, intermediates, and final products were observed on an SS-550 scanning electron microscope (Shimadzu, Japan). An SS-550-IC-type sputtering apparatus (Shimadzu, Japan) was used to coat the samples with gold prior to the experiments.

Thermal Properties Analysis

Thermogravimetric analysis (TGA) and differential scanning calorimetry (DSC) were performed with an STA 409PC simultaneous thermal analyzer (Netzsch, Germany) under a nitrogen atmosphere at 25 mL/min from 20 to 600°C and at a heating rate of 10°C/min. The quantity of the sample was 9.20–10.40 mg.

Biodegradability Measurement

Method of the Incubation Media with a Merely Carbon Source. The biodegradability of the reactants, intermediates, and end products was tested by the choice of *Trichoderma* spp. as strains of material degradation and the choice of a carbon-only source medium as the medium: fine powder sample = 0.15%, $MgSO_4{\cdot}7H_2O = 0.05\%$, $NH_4Cl = 0.1\%$, $CaCl_2{\cdot}2H_2O = 0.0005\%$, $KH_2PO_4 = 0.554\%$, and $Na_2HPO_4{\cdot}12H_2O = 1.194\%$. NaOH (0.01 mol/L) was used to adjust the culture medium to pH 6.8–7.0. Under sterile conditions, the strain materials were prepared as a solution containing 4.6×10^6/mL single *Trichoderma* spp. by means of the microscope. A quantity of the sample powder was sprinkled homogeneously on the incubation medium. Then, an asepsis gun was used to inoculate the strain in the middle of the incubation media. The treated incubation media was cultivated at 28°C in an oven. The growing formation of the fungus and the degradation rate of the sample were observed regularly. After a period of time, the degradation samples were taken out and rinsed carefully, and the degradation state was observed with scanning electronic

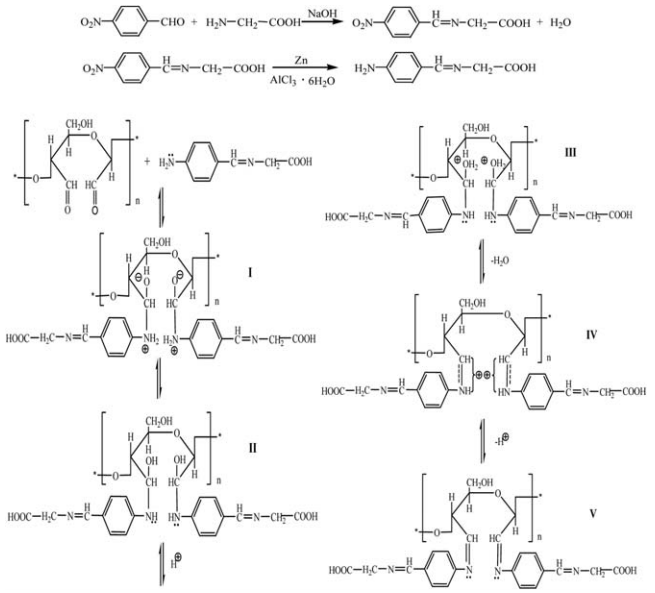

Figure 1. Synthesis scheme of DAC-*g*-Gly.

microscopy (SEM). At the same time, the microstructural changes in the reactant and product were compared and analyzed.

Method of the Active Sludge[15]. Some superficial garden soil was obtained, and its debris was removed. A slurry mud with a 50% moisture content was prepared after the soil was dried to a balanced weight, and the slurry mud was loaded into flask A after its pH was adjusted to 6.8 with a dilute $NaHCO_3$ solution; a 0.2 mol/L NaOH solution (200 mL) was added to flask B. An amount of 0.0125 g of DAC-*g*-Gly was introduced into flask A and shaken enough. Then, flasks A and B were connected with a closed tube. The experimental devices and contrast devices were placed in a constant-temperature incubator together at 30°C with regular oscillation. Four weeks later, flask B was taken out, and the NaOH solution was titrated by HCl with the phenolphthalein/methyl orange double-indicator titration method. For this titration method, with the phenolphthalein indicator, the endpoint volume of the HCl solution was recorded as V_1; with the methyl orange reagent consumption, the endpoint volume of HCl solution was recorded as V_2. The same operation was used for the contrast experiment, and the corresponding volumes were recorded as $V_{1'}$ and $V_{2'}$, respectively. The rate of degradation of the samples could be calculated according to the experimental data.

RESULTS AND DISCUSSION

Synthesis of DAC-*g*-Gly

Three steps were involved in the preparation of DAC-*g*-Gly. First, CF was treated with alkali swelling activation, and DAC was prepared by the selective oxidation of sodium periodate. Second, the *p*-NBD–Gly–Schiff base was synthesized by Gly and *p*-NBD, and aminobenzaldehyde Gly–Schiff base (*p*-ABD–Gly–Schiff base) was obtained by the reduction of the aromatic nitro groups of amino in the *p*-NBD–Gly–Schiff base. Then, the DAC-*g*-Gly product was obtained under appropriate conditions by the grafting of the *p*-ABD–Gly–Schiff base to the DAC. The reaction process is shown in Figure 1.

A Schiff base reaction is mainly composed of two stages of addition and condensation reactions. Figure 1 shows the process of DAC grafting onto the *p*-ABD–Gly–Schiff base. Intermediate **I,** which was formed by the nucleophilic nitrogen atom of the *p*-ABD–Gly–Schiff base molecules attacking electrophilic carbocation of the DAC molecule of aldehyde, was instable and formed adducts **II** by further reaction; this tended to be stable. In this process, the acid promoted the addition reaction, adduct **II** was protonated by the effect of the acid solution, and the molecule had two basic centers. The N atoms were protonated back to **I** by a reverse reaction; this had no significance. Compound **III,** which was formed by the immediate protonation of hydroxyl oxygen (reversibly), changed to have a positive charge. This was away from the field of the carbon ions (**IV**) after dehydration, and it tended to be stable. The intermediate **VI** immediately produced the product **V** by the condensation reaction after it lost a proton. In the intermediate **IV**, the primary amine reactions to the Schiff base occurred, but enamine did not form because it was much easier to separate protons from the nitrogen atom than to separate the *β*-carbon atom of the proton.[16,17] The nitrogen content and the grafting ratio (*G*%) of the DAC-*g*-Gly product were measured in accordance with the literature.[18,19] The results indicate that the samples' nitrogen content was 1.57% and *G*% was 11.6%.

Analysis of FTIR Spectroscopy

FTIR spectroscopy is of importance in the study of molecular structure. The width and intensity of the spectral bands and the position of the peaks are all sensitive to environmental changes and to conformations of macromolecules on the molecular level.[20] The FTIR spectra of the Gly, *p*-NBD, *p*-NBD–Gly–Schiff base (*p*-NBD–Gly–Schiff base), and *p*-ABD–Gly–Schiff base (*p*-ABD–Gly–Schiff base) were measured and analyzed as follows.

The absorption bands at 3116, 1589, 1427, 679, 1496, 1395, and 1327 cm^{-1} in the spectrum of Gly were assigned to the symmetric stretching vibrations of —NH_2, the antisymmetric stretching vibration peaks of —COO^-, the symmetric stretching vibrations of —COO^- (weak), the angle vibration of —COO^-, the angle vibration of —CH_2—, the plane rocking of —CH_2—, and the stretching vibrations of —C—OH, respectively. The bands at 1121 and 1041 cm^{-1} were the stretching vibration peaks of aliphatic primary amine C—N, and those at 928 and 891 cm^{-1} were the bending vibration peaks of —NH_2.

The absorption bands at 2847 and 1708 cm^{-1} in the spectrum of *p*-NBD were assigned to the vibration absorption of aldehyde C—H and the stretching vibrations of C═O in aromatic aldehydes. The band at 1602 cm^{-1} exhibited the stretching vibrations of a benzene ring C═C. The bands at 1533 and 1352 cm^{-1} were the asymmetric and symmetric stretching vibrations of the aromatic —NO_2.[21] The stretching vibration absorption of C—N in the spectrum of *p*-NBD was located at 1196, 817, and 734 cm^{-1} and showed the stretching vibrations of unsubstituted C—H in the benzene ring of the *p*-NBD molecules. The band at 675 cm^{-1} belonged to the bending

vibrations of the parasubstituted C—H in the benzene ring, the type of which could identify the substitutive type of benzene ring in the fingerprint area.

In the IR spectrum of the *p*-NBD–Gly–Schiff base, the broad and strong absorption at 3403 cm^{-1} was the absorption of crystal water located in the *p*-NBD–Gly–Schiff base. The absorption appearing at 3441 and 3129 cm^{-1} in the spectrum of the *p*-ABD–Gly–Schiff base was the asymmetric stretching of —NH_2; this showed that the nitro group was successfully reduced to an amino group. The C═N absorption at 1602 cm^{-1} in the *p*-NBD–Gly–Schiff base and *p*-ABD–Gly–Schiff base[22] showed that the target of Schiff base was successfully synthesized with *p*-NBD and Gly. The symmetric variable-angle vibration absorption peak of —NH_3^+ at 1471 cm^{-1} in the *p*-ABD–Gly–Schiff base indicated that the —NH_2 group occurred in the form of hydrochloride. The stretching vibration peak of aromatic C—N, appearing at 1346 cm^{-1} in the *p*-ABD–Gly–Schiff base, was stronger than that in the *p*-NBD–Gly–Schiff base at 1340 cm^{-1}. This indicated that the primary amine-specific C—N bond absorption peak in the aromatic (p–π conjugated with double-bond characteristics with a strong absorption) formed in the *p*-ABD–Gly–Schiff base. This showed that the —NH_2 group was successfully reduced in the *p*-ABD–Gly–Schiff base molecules. The vibration peak of the C—O of the Gly carboxyl group existed as —COONa in the *p*-NBD–Gly–Schiff base at 1096 cm^{-1} and was weaker than that peak at 1065 cm^{-1} in the *p*-ABD–Gly–Schiff base in the form of a carboxyl group (—COOH). The peaks at 923, 834, 917, and 852 cm^{-1} were the stretching vibration peak of unsubstituted C—H in the benzene ring of the *p*-NBD–Gly–Schiff base and *p*-ABD–Gly–Schiff base molecules, respectively, whereas the peaks at 669 and 627 cm^{-1} were the plane bending vibrations of the substitute —C—H on the benzene ring of the *p*-NBD–Gly–Schiff base and *p*-ABD–Gly–Schiff base molecules, respectively. The —COO^- groups of amino acid asymmetric stretching vibration peak (1600–1555 cm^{-1}) and symmetric stretching vibration peak (1430–1370 cm^{-1}) in the *p*-NBD–Gly–Schiff base and *p*-ABD–Gly–Schiff base overlapped or were covered up by peaks of other groups and were not obvious, and the asymmetric stretching peak (1550–1500 cm^{-1}) and symmetric stretching peak (1365–1330 cm^{-1}) of aromatic —NO_2 in the *p*-NBD–Gly–Schiff base were not obvious for the same reason.

The IR spectra of the CF, oxidized CF (DAC), and DAC-*g*-Gly are shown in Figure 2.

As shown in Figure 2, the absorption bands at 3397 and 3434 cm^{-1} represented the stretching vibrations of —OH in CF and DAC, respectively, whereas the absorption peak of the C—H of —CHO in DAC appeared at 3191 cm^{-1}. The absorption peaks at 2904 cm^{-1} was the —C—H stretching vibrations of the glucopyranosyl ring on the CF, whereas it shifted to 2954 cm^{-1} in DAC because of the —CHO group that formed. The absorptions at 1638 and 1639 cm^{-1} of CF and DAC, respectively, were the water absorption by the samples.[23] The free aldehyde group stretching vibrations at 1732 cm^{-1} and the semiacetal vibrations at 872 cm^{-1} in DAC proved the successful selective oxidation reaction of CF. The peaks at 1377 and 1395 cm^{-1} were the

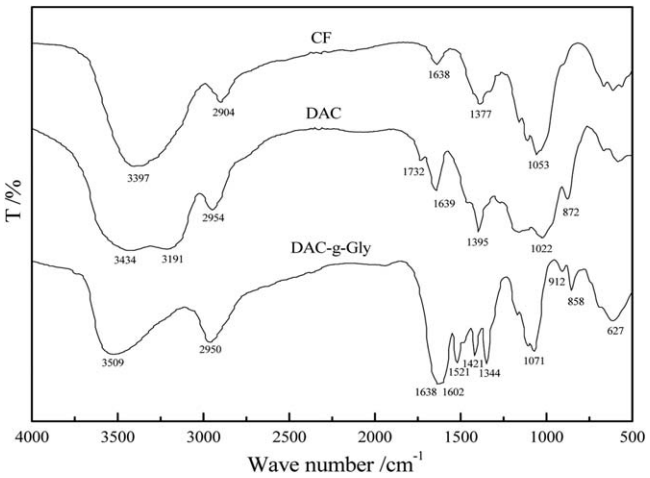

Figure 2. IR spectra of CF, DAC, and DAC-*g*-Gly.

plane rocking vibrations of —CH_2—. The peak of —CH—OH in the glucopyranosyl ring appeared at 1053 cm^{-1} in CF, whereas this vibration peak on DAC shifted to 1022 cm^{-1} and significantly decreased; this indicated that a part of —CH—OH in the glucose ring was oxidized to —CHO. Figure 2 also shows that the main structure of aldehyde, which was generated in the oxidation reaction of CF, was a hydrated semialdehyde alcohol and had intramolecular and intermolecular interactions within the semiacetal while the free form is very few.[24] Such potential semialdehydes and acetal aldehydes can occur in many reactions with acid or sulfite ions, alcohols, amines, hydrazines, acid reaction substances, and so on, so the oxidation of cellulose has a high chemical activity.[25,26]

As shown in Figure 2, the absorption peak of —OH shifted to 3509 cm^{-1}, and the vibration absorption peak of C—H in the glucopyranose ring shifted to 2950 cm^{-1} in DAC-*g*-Gly because of the grafting reaction, although a wide and strong absorption peak of —C═N— appeared from 1638 to 1602 cm^{-1}; this indicated that the *p*-ABD–Gly–Schiff base was successfully grafted onto the DAC. The C terminus and N terminus of phenyl formed the Schiff base structure, and the DAC-*g*-Gly molecules were successfully synthesized. The absorption band at 1344 cm^{-1} was the stretching vibrations of the aromatic C—N, that at 1071 cm^{-1} was the —C—O of the carboxyl group on the Gly, the bands at 912 and 858 cm^{-1} represented the unsubstituted C—H in benzene ring, and the peak at 627 cm^{-1} was the plane bending vibrations of the substituted C—H in the benzene ring. This typical structure of the benzene ring proved that the products of DAC-*g*-Gly were successfully prepared.

CP/MAS ^{13}C-NMR Analysis

CP/MAS NMR has become a powerful tool for studying the chemical structure and physical properties of polymers. ^{13}C-NMR is widely used.[27]

The CP/MAS ^{13}C-NMR spectra of the reactant (CF), DAC, and final product (DAC-*g*-Gly) are shown in Figure 3.

As shown in Figure 3(A), C_1, C_4, and C_6 on the glucose ring of CF split into two broads, one of which was narrow and sharp in a low field and the other of which was broad in a high field.

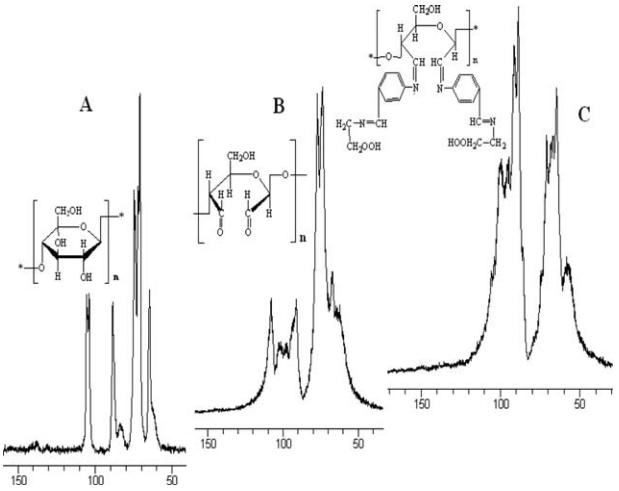

Figure 3. ^{13}C-NMR spectra of (A) CF, (B) DAC, and (C) DAC-*g*-Gly.

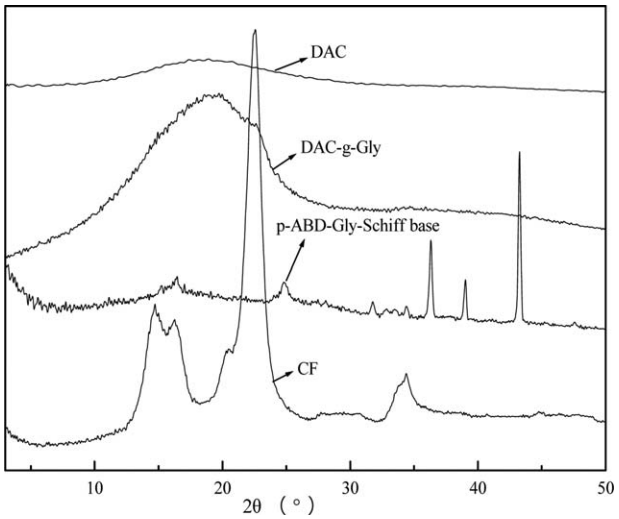

Figure 4. XRD spectra of CF, DAC, *p*-ABD–Gly–Schiff base, and DAC-*g*-Gly.

The δ values of 105.42, 103.69, 88.57, 83.75, 64.58, and 64.40 ppm corresponded to the chemical shifts of the C_1 crystallization zone, C_1 noncrystalline region, C_4 crystalline region, C_4 noncrystalline region, C_6 crystallization zone, and C_6 noncrystalline region, respectively. The strong overlapping absorption signal at $\delta = 70.99$–74.61 ppm were from the crystalline area and noncrystalline regions of C_2, C3, and C_5 on the glucose ring of CF.[28] As shown in Figure 3(B), the lack of an obvious, sharp, narrow crystallization peak in DAC indicated that the crystallization zone of CF was substantially destroyed after oxidation. With the presence of aldehyde in the oxidized CF, C_1, C_4, and C_6 had different shifts: $\delta = 96.18$–101.32 ppm was the absorption peak of C_1, $\delta = 87.40$–92.89 ppm was the absorption peak of C_4, and the small wide peak around $\delta = 61.32$ ppm was attributed to the absorption of C_6. The value at $\delta = 66.64$–73.06 ppm was the absorption peaks of the common overlapping of C_5 with the hydroxyl oxidation of C_2 and C_3 and the hydroxyl nonoxidation of C_2 and C_3 in DAC.[29,30]

For the ^{13}C-NMR spectrum of DAC-*g*-Gly, it was difficult to analyze the chemical shift alterations of C_2 and C_3 because of the overlapping peaks of C_2 and C_3 with C_5. Although the C_1, C_4 and C_6 chemical shifts overlapped relatively little and the cellulose molecules in the C_1 and C_4 had no free carbonyl positions, the chemical shifts of C_1 and C_4 certainly changed because of the adjacency of C_2, C_3 and C_1, C_4. The chemical shift of C_1 deviated to a low field was $\delta = 98.96$–94.64 ppm. The C_4 position in the high field was $\delta = 91.23$–85.58 ppm. The absorption peak of C_2, C3, and C_5 also shifted to $\delta = 71.07$–64.81 ppm. Two weak peaks were divided at the low field of C_6, which appeared at $\delta = 59.31$ and 58.32 ppm because of the Schiff base reaction of the amino benzaldehyde oxidation of Gly and DAC. The successfully prepared DAC-*g*-Gly was further confirmed by the CP/MAS ^{13}C-NMR spectrum.

XRD Analysis

It is common to determine the crystallinity of a polymer by XRD analysis, in which the crystallinity data can be obtained easily according to the sample diffraction data and computer subpeak software. The differences between the elements and functional groups of the graft polymer will lead to the diversification of the number of diffraction patterns, angle positions, and relative intensities of the order and shape of the diffraction peaks in the diffraction spectrum. Therefore, the sample phase composition and structural identification can be completed by comparison and analysis between the XRD patterns of the samples and the XRD patterns of known crystalline substances. Figure 4 shows the XRD curves of the CF, DAC, *p*-ABD–Gly–Schiff base, and DAC-*g*-Gly. The crystallinity (X_c) was calculated by eq. (1)[31] with computer subpeak software:

$$X_c(\%) = A_c/(A_c + KA_a) \times 100\% \quad (1)$$

where A_c is the area of diffraction of the crystalline peak in the XRD atlas, A_a is the area of the diffraction amorphous peak in the XRD atlas, and K is the correction factor.

As shown in Figure 4, there were some differences in the peak height, width, and position among these samples. CF had typical characteristics of cellulose. Its crystallinity was 63.7%, and the typical amorphous diffraction peaks at $2\theta = 14.6$, 16.2, and 34.4°, and the independent sharp crystalline peak at $2\theta = 22.5$ was in line with the characteristics that showed that there were crystalline and noncrystalline regions in the cellulose molecules. DAC had only one noncrystalline diffraction peak at $2\theta = 18.9°$; this indicated that when the oxidation reaction occurred, the oxidation reagent permeated and diffused to the inside of the cellulose chains, and the oxidation reaction extended from the surface of the crystal fibers to the inner crystalline regions. With the development of oxidation reactions, the number of opened dehydration glucose rings in the macromolecular chain of CF increased. The oxidation of cellulose gradually increased; this destroyed a large number of combinations of the original hydrogen bonds in the CF molecules and weakened the molecular interactions so that the cellulose molecule changed from a highly ordered arrangement to a disordered arrangement, and the crystalline region produced some stripping solution. Therefore, the crystallinity of DAC decreased to 22.2%. As shown in the *p*-ABD–Gly–Schiff base spectrum in Figure 4, two

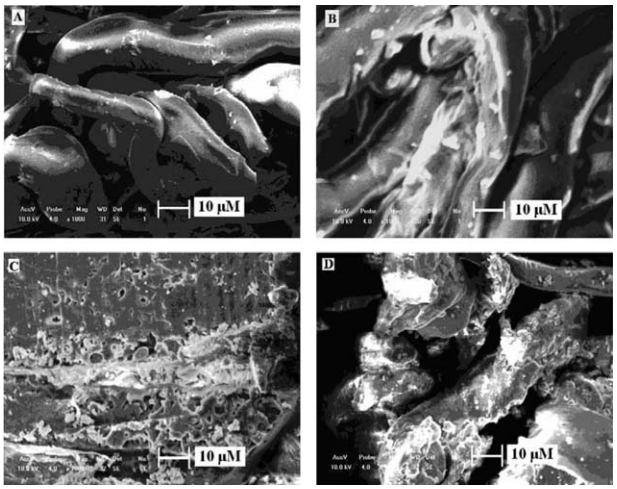

Figure 5. SEM of (A) CF, (B) DAC, (C) *p*-ABD–Gly, and (D) DAC-*g*-Gly (magnification: 1000 ×, $\delta = 10.0$ μm).

amorphous peaks at $2\theta = 16.5$ and 24.8° and three independent, sharp crystalline peaks at $2\theta = 36.3$, 39.1, and 43.3° coincided with semicrystalline small molecule compounds, and the crystallinity was 50.8%. DAC-*g*-Gly had a large and wide amorphous peak at $2\theta = 19.2°$, and its crystallinity was 46.4% after the *p*-ABD–Gly–Schiff base was grafted onto the skeleton of DAC in the form of a single molecule. The crystallinity of the overall structure of DAC increased because of the combination of Schiff base molecules. The reactive aldehyde in DAC formed imine bonds with the *p*-ABD–Gly–Schiff base and hydrogen bonds; this led to part of the DAC being restructured, the fiber macromolecules having an orderly arrangement, an increase in the regularity of the molecular chain segments, the internal structure of DAC becoming close, and an increasing trend in the crystallinity.

Analysis of the Surface Topography

SEM is one of the most significant tools used to observe surface topography of polymer materials. With a polymer grafting reaction, there is a corresponding change in the apparent structure of intermediates and final products, so the synthetic reaction can be confirmed, and the products can be characterized by the analysis of the surface topography. In this test, the surface topography of the CF, DAC, *p*-ABD–Gly–Schiff base, and DAC-*g*-Gly were observed with the SS-550 scanning electron microscope. Figure 5 shows the corresponding photos of SEM (with δ denoted as the unit of proportional scale, × denoting the magnification, and the number denoting as the multiples).

The surface of CF [Figure 5(A)] was very smooth, and its surface gloss was high. After selective oxidation, DAC [Figure 5(B)] retained the main structure of CF, but the main structure fractured because of oxidation, the length showed a decreasing trend, and the surface appeared to fold and revealed a number of microfibers. The surface of small molecules of the *p*-ABD–Gly–Schiff base [Figure 5(C)] had a disorderly scattered structure, and after the reaction, the DAC grafted onto the *p*-ABD–Gly–Schiff base, and the surface morphology [Figure 5(D)] underwent tremendous changes. There were obvious *p*-ABD–Gly–Schiff base molecules attached to the fiber surface, uneven distribution, and the oxidation of the overall structure of the CFs tended to be more loose. The apparent morphology underwent certain changes, which corresponded to changes in its structure; we could expect that the performance of the products would also undergo some changes.

Analysis of the Thermal Properties

TGA. TGA is currently an important method for researching the thermal characteristics of polymers. In practical applications, the thermal stability of cellulose and its derivatives important, and it has important referential meaning in the processing and formation, fusion characteristics, and mechanical properties of chemically modified cellulosic materials. In this study, the thermogravimetric experiments of the CF, DAC, *p*-ABD–Gly–Schiff base, and DAC-*g*-Gly were performed, and the thermal stability was analyzed. The corresponding measured data are listed in Table I.

The TGA and differential thermogravimetry (DTG) data of CF included three weight loss stages. The first stage was from room temperature to about 150°C, where the weight loss rate was 6.6%. This was mainly caused by the loss of free water and crystalline water. The second stage, in the 150–400°C temperature range, was the initial degradation stage of cellulose, in which the decomposition reaction played a dominant role, and the rupture and dehydration of the cellulose molecular chain occurred. In this stage, the feature of a rather large weight loss rate and a great magnitude of mass loss appeared (with a total loss of 59.7% of the mass, except in the first stage of dehydration), and most of the degradation products were produced in this stage. The third stage was located in the high-temperature range of 400–600°C. The residues were continuously cracked; namely, the remaining products originating from the initial degradation stage were continuously being decomposed (by dehydration, dehydrogenation, decarbonation, etc.), and the final char composition was formed in this stage (a 9.8% weight loss rate).

Table I. TG Data for CF, DAC, *p*-ABD–Gly–Schiff, and DAC-*g*-Gly

Sample	T_{dm} (°C)	T_{di} (°C)	T_{df} (°C)	Char yield at 600°C (wt %)
CF	348.5	142.4	563.1	23.90
DAC	333.2	155.1	551.2	35.20
p-ABD–Gly–Schiff base	230.8	173.5	370.9	68.10
DAC-*g*-Gly	436.1	220.1	503.2	44.80

T_{dm}, maximal weight loss temperature; T_{di}, initial weight loss temperature; T_{df}, final weight loss temperature.

The thermal decomposition of DAC could also be divided into three stages. The first stage was from room temperature to 150°C; this was caused by the loss of water as in CF. The weight loss rate increased slightly, up to 8.7%, and the maximum temperature of dehydration was higher than that of CF. This was mainly attributed to the formation of hemiacetal between the water molecules and the aldehyde in DAC molecule. The binding of the water molecule in the form of hemiacetal was stronger than the binding of the water molecule in the form of hydrogen bonds in the CF molecule, and the water content of DAC was also greater. The temperature range of the second phase was 150–450°C. The mass loss was about 51.3%; this may have been related to the destruction of the fiber crystal structure of DAC and the change in the state of amorphous DAC. It was also clear from the DTG data that the biggest thermal decomposition temperature of DAC was lower than that of CF at this stage. This was because the bonding energy of aldehyde was lower, and it was more easily broken to produce small molecules by thermal degradation. These small molecules left the system quickly and led to rapid weight loss in the system. The third stage was in the range 450–600°C, the mass loss was 4.8%, and the final char component was formed. The total weight loss of DAC was about 64.8% lower than that of CF (76.1%).

The XRD crystallinity of DAC decreased to 22.2% compared with the CF crystallinity of 63.7%. In the thermogravimetry (TG)/DTG curves, the weight losses of DAC were observed at 155.1, 333.2, and 551.2°C, whereas three peaks registered around 142.4, 348.5, and 563.1°C were observed for the CF sample. The biggest weight loss peak occurred in the second section, and the decomposition temperature decreased because of the oxidation reaction. This result of TG/DTG corresponded to the decrease in the crystallinity.

The TG and DTG data of DAC-*g*-Gly could be divided into four stages, and the characteristics of each stage were different. The first stage was from room temperature to 150°C, and the mass loss caused by water loss was 4.1%. The water molecules in the DAC-*g*-Gly sample mainly existed in the form of free water rather than hemiacetal water, so the maximum decomposition temperature and water content all decreased. The second stage was in the range 150–400°C, and the mass loss was 39.9%. The maximum thermal decomposition temperature of this phase was lower than that of the DAC, and this may have been due to the entire destruction of the polymer crystal structure, which resulted in the more easy degradation of the molecular chain degradation. Also, the formation of the Schiff base contained unsaturated C═N bonds, which made it easier for the molecule to form a volatile material. The third temperature stage, from 400 to 450°C, was the thermal condensation stage, and the mass loss was 7.9%; this was mainly caused by the thermal condensation reaction of organic components in the samples.[32] The fourth stage was located in the range 450–600°C. The mass loss was 3.3%, and the char composition was finally formed. The total mass loss of DAC-*g*-Gly was 55.2%; this was lower than those of DAC (64.8%) and CF (76.1%). This may have been due to the more stable aromatic ring structure involved in the polymer. The XRD experiments revealed that the DAC crystallinity was lower, as compared with CF, and the structure of the cellulose molecule changed from ordered to disordered. The crystalline region was disrupted and produced stripping and dissolution to a certain extent. The TG and DTG data show that the degraded and less crystalline DAC had a higher char yield than CF; this could be described as follows. During the thermal degradation process of the cellulose molecule chain, the rearrangement, crosslinking, and depolymerization reactions of the molecules may have occurred, and the aldehyde group of the oxidized cellulose may also have formed new hydrogen bond and the hemiacetal with the hydroxyl group of the cellulose macromolecules. This led the molecular chain to recombine and form a new crystalline structure. At the same time, some large crystals were destroyed, and the rest of the small crystals rearranged into a more fine and uniform aggregation structures of fibers; this changed the ordered structure of cellulose and produced the recrystallization process so that the residual carbon content of the oxidized cellulose was relatively high. The oxidized cellulose samples, when heated, gave rise to high char yields; this was also observed in the literature, and the relevant studies had a number of results consistent with our own.[33–36]

It could be analyzed from the TG and DTG data of the CF, DAC, and DAC-*g*-Gly that the mechanism of weight loss became very complex after a series of reactions of activation, oxidation, and grafting, and further analysis is given as follows and combined with the X-ray data. The CF macromolecular chain was depolymerized, and it was partially degraded into oligomers after CF was selectively oxidized by sodium periodate. The interactions among the intermolecular chains were greatly weakened, and this decreased the crystallinity. The severely damaged crystal structure of DAC weakened the force of binding-chain segment movement, and the degree of molecular freedom increased. At the same time, the introduction of the active aldehyde group to the DAC molecule skeleton formed hydrogen bonds and a semiacetal structure. The chain segments could be repiled after the grafting of the *p*-ABD–Gly–Schiff base, and the molecular chains were recrystallized. Then, the thermal stability was improved as a result. Therefore, there were corresponding molecular structural changes between the crystalline structure, the transition-state structure, and the amorphous structure at different polymer grafting reaction stages along with the synthesis progress. During the whole process, a more complicated decomposition model (peak) appears, and it showed a thermodynamic nature.

DSC Analysis. DSC is an analytical method that measures the differences in power between a sample and a reference compound, with temperature relations keeping the sample at the same conditions as the reference compound in a temperature-controlled program. The measured DSC data of the CF, DAC, *p*-ABD–Gly–Schiff base, and DAC-*g*-Gly are listed in Table II.

From the DSC measurement, CF had two distinct melting endothermic peaks in the temperature range 400–600°C, whereas the DAC had only one melting endothermic peak at a lower temperature than CF; this indicated that the chemical bond of C_2–C_3 located in the glucopyranosyl ring was broken in the oxidation reaction process of CF, and the multilevel

Table II. DSC Data for the Raw Material, Intermediate Material, and Final Product

Sample	Initial melting (°C)	Endothermic melting peak width (°C)	Peak temperature (°C)
CF	259.1	378.6-471.1, 485.6-580.8	561.4
DAC	257.1	460.3-589.2	547.8
p-ABD-Gly	297.9	336.8-466.2, 484.7-556.6	407.9
DAC-*g*-Gly	246.4	378.7-481.7, 481.8-591.6	564.4

polymer structure of CF was damaged and degraded. The whole structure of DAC was looser, and the crystallinity was lower compared with CF. Therefore, the melting temperature and thermal stability of DAC was reduced in comparison to that of CF.

DAC-*g*-Gly had two melting endothermic peaks in the temperature range 400–600°C: one was the largest melting endothermic peak of the *p*-ABD–Gly–Schiff base substructure in the graft product, and the other was the melting endothermic peak of the DAC skeleton. The melting point of DAC-*g*-Gly was higher than that of DAC; this was related to the increase in the crystallinity and the intensity in the internal fiber structure after the *p*-ABD–Gly–Schiff base was grafted onto DAC.

Analysis of the Biodegradability

Biological Degradation Analysis by Incubation Media with Only a Carbon Source. SEM is an effective method among all of the evaluation methods for evaluating the biodegradability of a modified polymer. The infection status of a polymer by microorganisms can be observed with SEM, and the biodegradability can be determined by changes in the apparent morphology of the polymer. In this test, the surface topographies of the CF, DAC, and DAC-*g*-Gly, which endured degradation experiments by *Trichoderma* spp., were observed with SEM. Figure 6 shows the corresponding SEM photos.

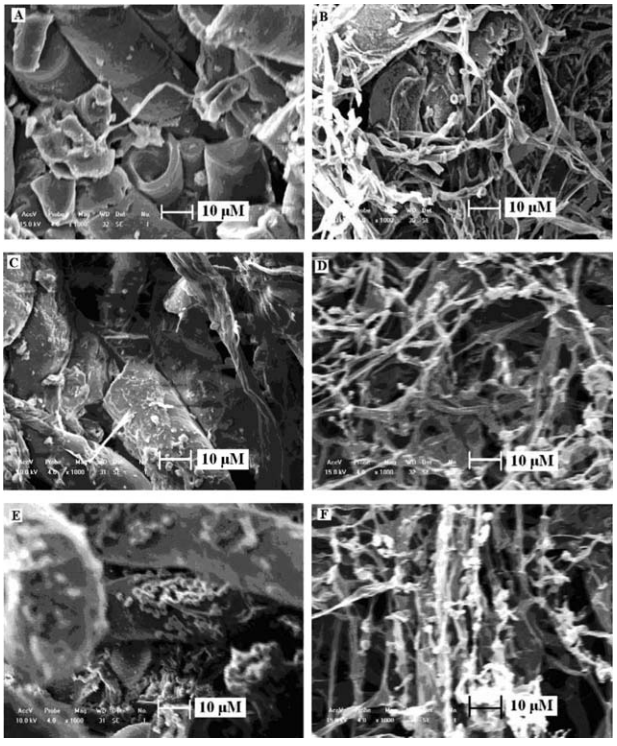

Figure 6. SEM of (A) CF after 7 days, (B) CF after 14 days, (C) DAC after 7 days, (D) DAC after 14 days, (E) DAC-*g*-Gly after 7 days, and (F) DAC-*g*-Gly after 14 days (magnification: 1000 ×, $\delta = 10.0$ μm).

After 1 week of microbiological deterioration, the green of *Trichoderma* spp. colony was observed on the incubation media when the samples of CF, DAC, and DAC-*g*-Gly were used as the only carbon source; however, the contrast sample showed a blank phenomenon. The volume of the colony increased with the proliferation of fungi after 2 weeks of the experimental treatment.

Figure 6(A–F) shows the SEM photos of microbiological deterioration after 1 and 2 weeks. The sample was carefully washed. Sterile water was used to wash it three times. Then, it was put into 0.2% mercuric chloride to soak and clean it for 5 min. Sterile water was used to wash it three times again, and then, it was put into 75% alcohol for 30 s. Sterile water was used to wash it three times again for the last time. However, the bacterial filament on the surface of the samples could still be seen, and the mycelium invaded the inside of the material, especially after the samples was trained for 14 days. As shown in the SEM photos, small crushed grain and crack on the surface of the sample could also be observed at the end of 7 days. What is more, the crevice on the surface of the sample was more conspicuous after 14 days of experiment treatment. This showed that *Trichoderma* spp. could grow on the incubation media with the provided sample as the single carbon source. In other words, the synthetic grafting copolymer (DAC-*g*-Gly) also possessed biodegradability after the *p*-ABD–Gly–Schiff base was grafted onto the skeleton of cellulose. In a comparison of Figure 6(B) with Figure 6(D) and Figure 6(F), it can be seen that the degree of degradation (*D*%) of DAC and DAC-*g*-Gly was severe more than that of CF, whereas the difference between DAC and DAC-*g*-Gly was not obvious. This fact shows that the oxidation had an impact on the structure of CF, whereas its crystalline region was destroyed, its structure was loose and disordered, and degradation had occurred in the oxidation process of CF. So, DAC was more easily eroded by microorganisms. The results were consistent with the previous findings from the IR and X-ray spectra. As shown in the SEM photos, we found that DAC-*g*-Gly and DAC had the same notable biodegradability from comparing their surfaces in the degradation process.

Biological Degradation Analysis by the Active Sludge. Equation (2) was used to determinate the concentration of the mixed

alkali Na_2CO_3 with the double-indicator method. The concentration of Na_2CO_3 (M_1) in the absorption bottle (B) could be calculated with eq. (2) when the samples were degraded for 4 weeks by the active sludge. Equation (3) was used to calculate the concentration of NaOH (M_2) in the absorption bottle when the samples were degraded for 4 weeks:

$$M_1 = \frac{(V_2 - V_1 + V_1' - V_2')c}{2V} \times 100\% \quad (2)$$

$$M_2 = \frac{(2V_1 - V_2)c}{V} \times 100\% \quad (3)$$

where c is the concentration of titration HCl, V is the volume of the mixed fluid, V_1 is the volume of the consumed HCl solution at the endpoint indicated by phenolphthalein, V_2 is the volume of the consumed HCl solution at the endpoint indicated by methyl orange, V_1' is the volume of consumed HCl solution at the phenolphthalein endpoint for the blank experiment, and V_2' is the volume of the consumed HCl solution at the methyl orange endpoint for the blank experiment. According to eqs. (2) and (3), M_1 was calculated as 2.1×10^{-3} mol/L, and M_2 was calculated as 0.1556 mol/L.

The percentage carbon content (C%) of DAC-*g*-Gly was calculated according to eq. (4):

$$C\% = G\% \times 60.7\% + (1 - G\%) \times 45.0\% \quad (4)$$

where the mass fraction of carbon in the DAC molecule was 45.0% and the mass fraction of carbon in the *p*-ABD–Gly–Schiff base was 60.70%. G% of the *p*-ABD–Gly–Schiff base with DAC was calculated with the weight data of raw materials and product in this experiment and was 11.6%. Thus, C% of DAC-*g*-Gly was obtained as 46.8% with eq. (4). D% of DAC-*g*-Gly was calculated with eq. (5):

$$D\% = \frac{(V_2 - V_1 + V_1' - V_2')cM_c}{Cm_0 \times 1000} \times 100\% \quad (5)$$

where m_0 is the initial weight of DAC-*g*-Gly and M_c is the molar mass of carbon. The experimental data were used to calculate the D% value, and the result was 9.91% according to eq. (5). This means that the degradation rate of DAC-*g*-Gly was about 9.91% in sludgelike neutral soil that had a natural activity.

CONCLUSIONS

In this study, the bridge-connection function of a grafting bridge molecule was skillfully used according to a designed synthetic route. We presynthesized a *p*-ABD–Gly–Schiff base, making use of the Schiff base reaction of *p*-NBD with Gly. Then, *p*-ABD–Gly was introduced onto the DAC molecule under suitable conditions, and a novel cellulose-based material of DAC-*g*-Gly was successfully prepared by a three-step grafting method for the first time. The characterization was carefully performed by FTIR spectroscopy, XRD, CP/MAS ^{13}C-NMR, and SEM, and the results indicate that the structure of the samples was changed along with the synthetic route. The TGA and DSC tests showed that the reactant, the intermediate product, and the graft copolymer possessed different thermal stabilities, and their thermal behavior characteristics were met with the process of the synthetic reaction. The measurement of biodegradation showed that the biodegradability of DAC-*g*-Gly changed remarkably compared with the raw materials after a given degradation time by *Trichoderma* spp. The obtained degradation rate indicated that the biodegradability of the synthetic graft copolymer (DAC-*g*-Gly) was adequate, and it exhibited an appropriate biodegradation speed. This means that it may be to provide a potential environmentally friendly material in the future.

The results from our work may help to explain the synthesis of a kind of new cellulose-based Schiff base derivative. We also look forward to a further exploration of the properties of cellulose-based Schiff bases derivatives in subsequent work. We also hope more of these kinds of biodegradable biomaterial matrix materials can be prepared in future research.

ACKNOWLEDGMENTS

This work was supported by the Zhejiang Provincial Natural Science Foundation (contract grant number Y5090179); the Pre-Research Project of Research Center of Biomass Resource Utilization, Zhejiang A & F University (contract grant number 2013SWZ02-1); and the Pre-Research Project of Zhejiang A & F University (contract grant number 2010FK056).

REFERENCES

1. Gross, R. A.; Kalra, B. *Science* **2002**, *297*, 803.
2. Wojnárovits, L.; Földváry, C. M.; Takács, E. *Radiat. Phys. Chem.* **2010**, *79*, 848.
3. Dhar, N.; Akhlaghi, S. P.; Tam, K. C. *Carbohydr. Res.* **2012**, *87*, 101.
4. Sudeshd, K.; Dungania, R.; Jawaidb, M. *Carbohydr. Polym.* **2014**, *99*, 649.
5. Li, W.; Li, X. Y.; Wang, Q.; Pan, Y. J.; Wang, T.; Wang, H. Q.; Song, R.; Deng, H. B. *Carbohydr. Polym.* **2014**, *99*, 218.
6. Xin, S. J.; Li, X. Y.; Wang, Q.; Huang, R.; Xu, X. L.; Lei, Z. J.; Deng, H. B. *J. Biomed. Nanotechnol.* **2014**, *10*, 803.
7. Peltzer, M.; Pei, A. H.; Zhou, Q.; Berglund, L.; Jiménez, A. *Polym. Int.* **2014**, *63*, 1056.
8. Binder, C. F.; Thomas, B. *Carbohydr. Polym.* **2012**, *90*, 937.
9. Jin, X. X.; Wang, J. T.; Bai, J. *Carbohydr. Res.* **2009**, *344*, 825.
10. Sachse, A.; Mösch-Zanetti, N. C.; Lyashenko, G.; Wielandt, J. W.; Most, K.; Magull, J. *Inorg. Chem.* **2007**, *46*, 7129.
11. Jiang, Y. M.; Zhang, S. H.; Xu, Q.; Xiao, Y. *Acta Chim. Sinica* **2003**, *61*, 573.
12. Wu, X. H.; Gorden, A. E. V. *J. Comb. Chem.* **2007**, *9*, 601.
13. Dohno, C.; Okamoto, A.; Saito, I. *J. Am. Chem. Soc.* **2005**, *127*, 16681.
14. Kanth, S. V.; Ramaraj, A.; Rao, J. R.; Nair, B. U. *Process. Biochem.* **2009**, *44*, 869.
15. Guo, M.; Wang, P.; Wang, C. P.; Chu, F. X. *Polym. Mater. Sci. Eng.* **2009**, *25*, 120.

16. Nyarku, S. K.; Mavuso, E. *South Africa J. Chem.* **1998**, *51*, 168.
17. Send, R.; Sundholm, D.; Johansson, M. P.; Pawłowski, F. *J. Chem. Theory Comput.* **2009**, *5*, 2401.
18. Yin, Q. F. PhD thesis, Dalian University of Technology, **2007**.
19. Guo, M.; Meng, H. W.; Wang, P.; Wang, C. P.; Chu, F. X. *Asian J. Chem.* **2010**, *22*, 1415.
20. Weng, S. F. Fourier Transform Infrared Spectroscopy; Beijing: Chemical Industry Press, **2005**.
21. Wu, G.; Mason, P.; Mo, X.; Terkikh, V. *J. Phys. Chem. B* **2008**, *112*, 1024.
22. Schwab, M. G.; Fassbender, B.; Spiess, H. W.; Thomas, A.; Feng, X. L.; Müllen, K. *J. Am. Chem. Soc.* **2009**, *131*, 7216.
23. Hou, Q. X.; Liu, W.; Liu, Z. H.; Bai, L. L. *Ind. Eng. Chem. Res.* **2007**, *46*, 7830.
24. Islam, N.; Haque, M.; Huque, M. *Ind. Eng. Chem. Res.* **2009**, *48*, 10491.
25. Joseleau, J. P.; Chevalier-Billosta, V.; Ruel, K. *Biomacromolecules* **2008**, *9*, 767.
26. Shi, L.; Zhen, W. J.; Shan, Z. H. *Fine Chemicals* **2008**, *25*, 795.
27. Nakazawa, Y.; Asakura, T. *Macromolecules* **2002**, *35*, 2393.
28. Husson, E.; Buchoux, S.; Avondo, C.; Cailleu, D.; Djellab, K.; Gosselin, I. *Bioresour. Technol.* **2011**, *102*, 7335.
29. David, K.; Pu, Y. Q.; Foston, M.; Muzzy, J.; Ragauskas, A. *Energy Fuels* **2009**, *23*, 498.
30. Tan, I.; Flanagan, B. M.; Halley, P. J.; Whittaker, A. K.; Gidley, M. *J. Biomacromolecules* **2007**, *8*, 885.
31. Xiao, C. B.; Lu, Y. S.; Liu, H. J.; Zhang, L. N. *J. Appl. Polym. Sci.* **2001**, *80*, 26.
32. Cyras, V. P.; Commisso, M. S.; Mauri, A. N.; Vázquez, A. *J. Appl. Polym. Sci.* **2007**, *106*, 749.
33. Varma, A. J.; Chavan, V. B. *Cellulose* **1995**, *2*, 41.
34. Cao, X. W.; Ding, B.; Yu, J. Y.; Al-Deyab, S. S. *Carbohydr. Polym.* **2012**, *90*, 1075.
35. Dagmara, O.; Halina, K.; Alina, S. *Thermochim. Acta* **2004**, *418*, 123.
36. Huang, M.; Li, X. G. *J. Appl. Polym. Sci.* **1998**, *68*, 293.